

# Energy & Environmental Science

Accepted Manuscript



This is an *Accepted Manuscript*, which has been through the Royal Society of Chemistry peer review process and has been accepted for publication.

*Accepted Manuscripts* are published online shortly after acceptance, before technical editing, formatting and proof reading. Using this free service, authors can make their results available to the community, in citable form, before we publish the edited article. We will replace this *Accepted Manuscript* with the edited and formatted *Advance Article* as soon as it is available.

You can find more information about *Accepted Manuscripts* in the [Information for Authors](#).

Please note that technical editing may introduce minor changes to the text and/or graphics, which may alter content. The journal's standard [Terms & Conditions](#) and the [Ethical guidelines](#) still apply. In no event shall the Royal Society of Chemistry be held responsible for any errors or omissions in this *Accepted Manuscript* or any consequences arising from the use of any information it contains.

Cite this: DOI: 10.1039/c0xx00000x

www.rsc.org/xxxxxx

## N-doped Graphene Quantum Sheets on Silicon Nanowire Photocathode for Hydrogen Production

Uk Sim<sup>a,†</sup>, Joonhee Moon<sup>b,†</sup>, Junghyun An<sup>a</sup>, Jin Hyoun Kang<sup>b</sup>, Sung Eun Jerng<sup>a</sup>, Junsang Moon<sup>a</sup>, Sung-Pyo Cho<sup>b,c</sup>, Byung Hee Hong<sup>b,d\*</sup>, and Ki Tae Nam<sup>a\*</sup>

<sup>5</sup> Received (in XXX, XXX) Xth XXXXXXXXXX 20XX, Accepted Xth XXXXXXXXXX 20XX

DOI: 10.1039/b000000x

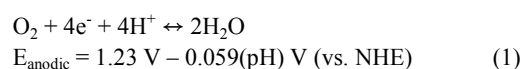
Photoelectrochemical hydrogen production from solar energy has been attracting much attention in the field of renewable energy technology. The realization of cost-effective hydrogen production by water splitting requires electrolysis or photoelectrochemical cells decorated with highly efficient co-catalysts. A critical requirement for catalysts in the photoelectrochemical cells is not only the ability to boost the kinetics of a chemical reaction but also to exhibit durability against electrochemical and photoinduced degradation. In the race to replace previous noble-metal catalysts, the design of carbon-based catalysts represents an important research direction in the search for non-precious, environmentally benign, and corrosion-resistant catalysts. Herein, we suggest graphene quantum sheets as a catalyst for the solar-driven hydrogen evolution reaction on Si nanowire photocathodes. The optimum nanostructures for the Si photocathodes exhibit an enhanced photocurrent and a lower overpotential compared to those of a planar Si surface. This significant enhancement demonstrates how graphene quantum sheet catalysts can be used to produce Si nanowire photocathodes as hydrogen evolution reaction catalysts with high activity.

### Introduction

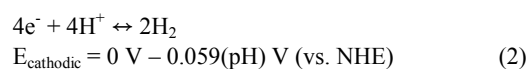
The development of sustainable energy sources is an urgent issue because of the current level of energy consumption.<sup>1</sup> Renewable and sustainable energy sources must be developed because present energy sources have several disadvantages such as CO<sub>2</sub> emission and limited deposits of fossil fuels.<sup>2</sup> Photoelectrochemical hydrogen production using solar energy represents an important and environmentally friendly technology with no carbon emissions.<sup>3</sup> The development of efficient and cheap photoelectrodes for water splitting is one of the fundamental challenges in hydrogen production.<sup>4</sup> Despite the intriguing advances in controlling the nanostructural interface and newly discovered material compositions for photoelectrodes, sluggish kinetic issues associated with a high overpotential remain some of the most difficult issues that need to be resolved.<sup>5, 6</sup> Intense research into efficient, durable, and inexpensive hydrogen evolution reaction (HER) catalysts has been undertaken to solve the kinetic problem.<sup>7-10</sup> In general, precious metals such as platinum exhibit superior performance HER catalysts; however, the unavoidable weakness of precious metals is their high cost.<sup>11</sup> A critical requirement for producing outstanding catalysts in a photoelectrochemical cell is not only the ability to boost the kinetics of electrochemical reaction but also the ability to resist electrochemical and photoinduced degradation. Herein, we demonstrate that the combination of

controlling a nanostructure of the photoelectrode and using a carbon-based hydrogen evolution catalyst represents a significant step toward enhancing the applied bias photon-to-current efficiency (ABPE). In the present work, a 430 mV decrease in overpotential was achieved using graphene quantum sheets on a silicon nanowire, which exhibited an enhancing effect comparable to that of platinum catalysts. Furthermore, the current density at the reversible potential vs. a reversible hydrogen electrode (RHE) exhibited a 101 fold enhancement relative to the current density achieved with planar silicon substrates.

The thermodynamic potential of water splitting is 1.23 V, which is observed by subtracting the reduction reaction and oxidation reaction in the photoelectrochemical reaction of water. At the anode, the oxidation reaction in the electrolysis of water is:



whereas the reduction reaction at the cathode is:



where, NHE is the normal hydrogen electrode and the standard potential is dependent on pH ( $E_{\text{half}} = E - 0.059(\text{pH})$  vs NHE). Kinetically, however, when a voltage of 1.23 V is applied, electrolysis is difficult to induce, which results in no current flow.

In this situation, a higher potential, which is referred to as the overpotential,  $\eta$ , is needed to drive the reaction at a certain rate. Moreover, if a current  $i_c$  flows at the cathode, a current  $i_a$  of the same magnitude must flow at the anode to complete the circuit, which requires the overpotential at both electrodes. The overpotentials at the cathode and anode are denoted as  $\eta_c$  and  $\eta_a$ , respectively. Therefore, the total applied potential,  $E_{\text{appl}}$ , is

$$E_{\text{appl}} = 1.23 \text{ V} + \eta_c + \eta_a \quad (3)$$

A higher overpotential requires a higher total applied voltage. Using an electrocatalyst for water splitting can reduce the overpotential required for the electrolysis of water.

In an effort to reduce the overpotential for the water splitting reaction, various catalysts have been deposited onto photoelectrode materials. Previously reported HER catalysts include pure metals, metal composites/alloys, compounds such as nonmetallic elements, and molecular catalysts. Among metal-based catalysts, Pt, Pd, and Ru are near the top of the volcano plot, exhibiting high catalytic activity toward the HER. For example, Pt nanoparticles on p-type Si nanowires in aqueous electrolyte solutions can enhance the onset potential by approximately 0.42 V. In view of economic issues, recent progress has been concentrated on the incorporation of metal nanoparticles into earth-abundant elements rather than on the use of noble metals alone. Nonprecious metal catalysts and catalysts that are abundant in nature have also exhibited high activity toward the HER. Binary structures such as  $\text{MoS}_2$ ,  $\text{Mo}_2\text{N}$ ,  $\text{Mo}_2\text{C}$ , and  $\text{Ni}_2\text{P}$  and bimetallic compounds such as Co-Mo-N and Ni-Mo have been suggested as catalysts with high HER activity. However, the rigorous and precise tuning of the composition of  $\text{A}_x\text{B}_y\text{M}_z$  compounds, controlling the active sites in catalysts for the HER, and nanostructuring make optimization of the properties of catalysts for the HER difficult. Moreover, when deposited with catalysts, the saturation current density and the current density at a reversible potential vs. RHE significantly decrease because of light scattering by catalysts on the surface of the photoelectrodes.

To solve the problems associated with previously developed catalysts, carbon-based catalysts may represent an important research direction in the search for low-cost, environmentally friendly, and corrosion-resistant catalysts. Among carbon-based catalysts, graphene, in particular, possesses excellent transmittance and superior intrinsic carrier mobility; thus, several attempts have been made to use graphene as a catalyst. Co-activated N and P heteroatoms adjacent to C atoms in the graphene matrix can affect such catalysts' valence orbital energy levels and thereby enhance their reactivity toward the HER. Graphitic-carbon nitride combined nitrogen-doped graphene also exhibits enhanced HER activity, with HER properties similar to those of well-established metallic catalysts. Reduced graphene oxide containing catalytic active materials has exhibited improved activity in oxygen reduction reactions and oxygen evolution reactions as well as in the HER. However, in most cases, the role of carbon materials is limited to an electrically conducting substrate or a supporter that increases the HER activity of other decorated active catalysts. Recently, we suggested that monolayer graphene deposited onto a planar Si

electrode acts as an efficient HER electrocatalyst and that  $\text{N}_2$  plasma treatment enhances its catalytic activity. In this study, we further investigated  $\text{N}_2$ -plasma-treated graphene quantum sheets deposited on the Si nanowire photocathodes as efficient HER electrocatalyst.

Controlling the surface structure of Si represents another important approach to improving photoelectrochemical performance. Si, one of the most abundant elements in the Earth's

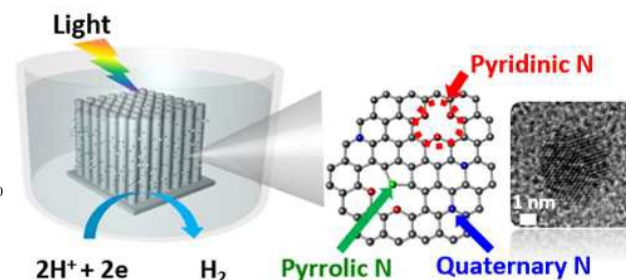


**Figure 1. Schematic of N-doped graphene quantum sheets (N-GQSs) decorated on a Si nanowire (SiNW) photocathode electrode.** Photons absorbed by the SiNWs generate minority carriers (electrons), which drift to the semiconductor/electrolyte interface, where  $2\text{H}^+$  is reduced to  $\text{H}_2$ ; the N-GQSs serve as electrocatalysts for hydrogen production. The gray, green, blue, and red spheres in the schematic of N-GQSs represent the carbon, pyrrolic nitrogen, quaternary nitrogen, and pyridinic nitrogen atoms, respectively. The average diameter of the N-GQSs is 5 nm, as determined from a TEM image.

crust, can be used both as a photocathode and a photoanode for photochemical water splitting because its bandgap (1.12 eV) allows for the absorption of a significant portion of the solar spectrum. However, the small band bending between the conduction band edge and  $\text{H}^+/\text{H}_2$  redox level of aqueous electrolytes limits the photoelectrochemical performance of Si relative to that of Si/non-aqueous solvent systems. The application of an external potential or the use of catalysts is necessary for efficient operation under solar irradiation. To overcome this problem, a porous structure or a nanostructure can increase the current density of Si photoelectrodes by increasing the number of effective reaction sites between the Si semiconductor and the liquid electrolyte junction as well as reducing the reflection of incident light. A nanowire structure can increase the efficiency due to the orthogonalization of the direction of incident light absorption and charge carrier collection. Therefore, the combination of an optimized Si nanowire photocathode and a graphene quantum sheet catalyst can boost the catalytic activity toward the photoelectrochemical HER.

## Results and Discussion

Measurements of photoelectrochemical performance show that N-doped graphene quantum sheets (N-GQSs) on Si photoelectrode exhibit catalytic HER activity. Figure 1 shows a schematic of hydrogen production on N-GQSs on Si nanowire arrays (SiNWs) in an acid solution under irradiation. Photons absorbed by the SiNWs generate minority carriers (electrons), which drift to the semiconductor/electrolyte interface where  $2\text{H}^+$  is reduced to  $\text{H}_2$ ; the N-GQSs serve as electrocatalysts for

Cite this: DOI: 10.1039/c0xx00000x

www.rsc.org/xxxxxx

## ARTICLE TYPE

hydrogen production. In the schematic of the N-GQSs, gray, green, blue, and red spheres represent carbon, pyrrolic nitrogen, quaternary nitrogen, and pyridinic nitrogen atoms, respectively, based on high resolution X-ray photoelectron spectrum (XPS) measurements. From Transmission electron microscopy (TEM) image and a size-distribution histogram indicate that the average diameter of the N-GQSs was 5 nm (Figure S1). N-GQSs were transferred to p-type silicon nanowires via drop-casting. The N-GQSs were converted from monolayer graphene on Cu foil using nitrogen plasma. After exposure to nitrogen plasma, the nano-sized GQSs were distributed on the Cu foil and were subsequently characterized by

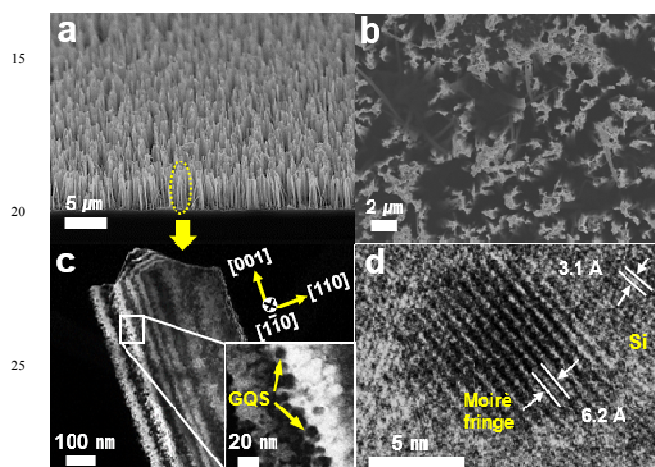


**Figure 2.** SEM images of SiNW arrays on p-silicon substrate obtained by metal assisted chemical etching method. (a) Cross-section and (b) top-view. (c) Dark-field TEM images of N-GQSs on p-SiNWs. (d) High-resolution TEM image shows Moiré pattern created by N-GQS in silicon lattices.

atomic force microscopy (AFM); the strong D peak of the sheets, which is related to the structural defects at the edges of graphene, was identified in the Raman spectrum. In addition, the doping of the GQSs with ~2.9% nitrogen was indicated by the N 1s XPS of the structures, and the UV-vis absorption spectrum of the N-GQSs revealed an absorption band with a peak at 275 nm, as shown in Figure S1. The well-aligned SiNW arrays serve as an anti-reflector that enhances light absorption in the structure and increases the overall surface area; the N-GQSs act as electrocatalysts for hydrogen evolution.

Top-view and cross-sectional scanning electron microscope (SEM) images of the N-GQSs on SiNWs are shown in Figures 2a and 2b. The SiNWs exhibited an average diameter of ~400 nm, and lengths of up to ~5 μm. To determine the crystallinity, orientation, and morphology of the N-GQSs on SiNWs, TEM analyses were performed. The selected area electron diffraction pattern, with an incident beam axis of [1-10] (Figure S3), indicated that a single-crystalline SiNW was well aligned along the [001] direction; the thickness fringes, brightness and dark line

pattern indicate that the SiNW was etched as a column with angled edges, as shown in Figure 2c. Moreover, the N-GQSs, which measured approximately 7 nm in diameter, were uniformly placed on the SiNWs, as indicated by dark-field TEM imaging (Figure 2c); moreover, the formation of the N-GQSs was verified by high-resolution TEM (HRTEM). The HRTEM image shows Moiré pattern created by the superposition of the mismatched crystalline lattices of the N-GQSs and SiNWs, as shown in Figure 2d. The lattice plane spacing of p-Si was observed to be 3.1 Å, which corresponds to the silicon (100) plane (JCPDS, No. 24-1402). The Moiré pattern (6.2 Å) indicates mixed translational and rotational geometry. The corresponding spacing of the fringes was calculated as follows.<sup>34</sup>

$$a_m = (a_{\text{GQS}} \times a_{\text{Si}}) / \sqrt{a_{\text{GQS}}^2 + a_{\text{Si}}^2 - 2a_{\text{GQS}}a_{\text{Si}}\cos(\alpha_{\text{GQS}} - \alpha_{\text{Si}})} \quad (4)$$

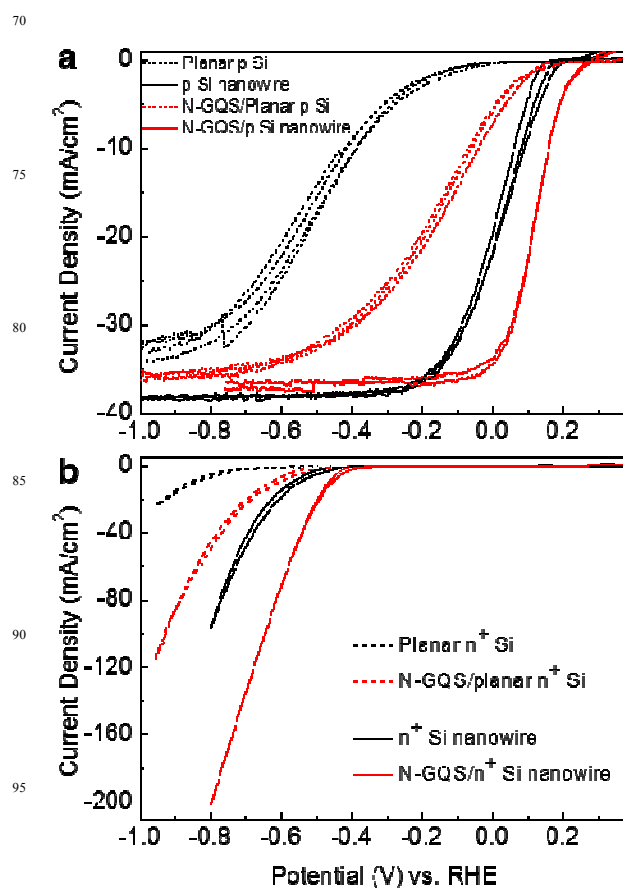


**Figure 3.** Cyclic voltammograms of N-doped graphene quantum sheets (N-GQSs) on silicon photocathodes. (a) Photocurrent density-potential ( $J$ - $E$ ) curves for a lightly boron-doped planar p-Si electrode and Si nanowire deposited with N-GQSs. The Si nanowire was fabricated using a metal-catalyzed electroless method. (b) Polarization curves of N-GQS on heavily arsenic-doped n<sup>+</sup>-type Si electrodes under dark conditions.

where  $a_m$  is the  $d$ -spacing of the Moiré pattern,  $a_{GQS}$  is the  $d$ -spacing of the N-GQS, and  $a_{Si}$  is the  $d$ -spacing of Si. On the basis of Eq. (4), the placement of an N-GQS on a SiNW with a 20 degree tilt was verified by the relation between the Moiré fringe spacing and the Si lattice plane.

To investigate the dependence of Si photoelectrode on its nanostructure, Si substrates of various nanostructures were fabricated by silver metal-assisted chemical etching.<sup>35</sup> Normal boron-doped p-type (100) Si substrates were immersed in an aqueous solution of 0.015 M silver nitrate and 5 M hydrofluoric acid. Continuous Si oxidation by the galvanic reduction of  $Ag^+$  ions and the ensuing dissolution of silicon oxide by HF resulted in the [100] directional etching of the Si substrates. The etching time was varied among 20 min, 30 min, 120 min, and 180 min. Depending on the etching time, different Si nanostructures were observed as characterized by SEM (Figure S5). When the etching time was shorter than 120 min, a porous nanostructure was observed. The transition of the surface structure from a porous to a nanowire structure occurred when the Si substrates were etched for 120 min. After this stage, the length of the nanowires was observed to increase with increasing etching time. Representative images of the SiNWs are shown in Figures 2a and 2b.

For the evaluation of the photocathodic behavior of the nanostructured Si electrodes, the current density was measured as the potential was swept from 0.4 V to -1.0 V vs. RHE in a three-electrode cell. A 300 W Xe lamp illuminated the Si photoelectrode with a light intensity of 100 mW/cm<sup>2</sup> through an Air Mass 1.5 Global filter in an aqueous 1 M perchloric ( $HClO_4$ ) acid solution (pH 0). Because the applied potential of the Si working electrode was negative (cathodic), the magnitude of the current density increased and saturated at a specific value of the applied potential. The current density at the saturation point is called the limiting current density or the saturation current density. As shown in Figure 3a and Figure S4, the current density of the planar Si continued to increase until the length of the nanowires reached 5  $\mu m$  as the surface became increasingly nanostructured. The limiting current density of bare planar Si was approximately -33 mA/cm<sup>2</sup>. The surface area of the nanostructured Si substrate was greater than that of the planar structure. The reflectance of incident light could be reduced by the nanostructured Si surface. Although the surface of planar Si reflects approximately one quarter of incident light, photon absorption is enhanced at the nanostructured surface because of its low reflectance. Nanostructured silicon wires have been reported to exhibit a light trapping effect,<sup>36</sup> which can enhance the current level for hydrogen production when the length of the Si nanowires is optimized to exhibit strong broadband optical absorption.<sup>37</sup> The nanowire structure also has the advantage of inducing the orthogonalization of light absorption and charge-carrier collection.<sup>33</sup> Thus, the minority carriers generated by incident solar light can move to the lateral side of each nanowire and participate in the hydrogen evolution reaction more quickly than in the planar structure. To calculate the photovoltage of the Si photoelectrode, the dark current density was also measured. The photovoltage is defined as the difference between the onset potential under the dark and illuminated conditions. Figure 2b shows the dark current densities of representative Si electrodes. The dark current density of the nanostructured electrodes was

also greater than that of the planar Si substrate. The nanostructured photoelectrode (0.59 V of photovoltage) exhibited a positive shift in photovoltage of 0.13 V relative to that of the planar Si electrode (0.46 V of photovoltage) as shown in Table S1.

In measurements of the photoelectro-catalytic performance, N-GQSs on SiNWs exhibited catalytic activity toward the HER. As shown in Figure 3a, the current density of the N-GQSs/planar Si structure increased gradually from -0.2 V vs. RHE and was saturated at approximately -35 mA/cm<sup>2</sup> below -0.8 V vs. RHE at negative applied potentials. This current density is higher than that of planar Si without N-GQSs. Interestingly, measurements of the N-GQSs/planar Si structure showed that the overall current density-potential ( $J$ - $E$ ) curve was shifted by approximately 0.2 V toward positive potentials compared to that of planar Si without N-GQSs. The onset potential is defined as the potential at a

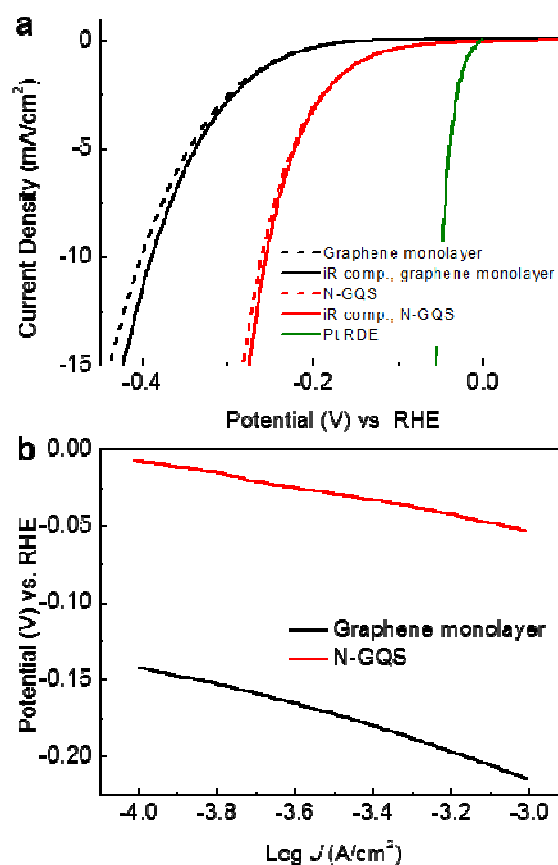


**Figure 4. Electrochemical activity of graphene monolayer and N-GQSs on glassy carbon (GC) electrodes in a rotating disk electrode system. (a) Cyclic voltammograms (CV) of a graphene monolayer on GC, N-GQSs on GC, Pt/C on GC. CV data obtained compensating for ohmic drop (iR) losses are also plotted (dashed curves). (b) Tafel plots derived from the CV data in (a).**

photocurrent density of -1 mA/cm<sup>2</sup>. The onset potential of N-GQSs/planar Si was 0.13 V vs. RHE, representing a positive shift of 0.30 V compared to the onset potential of bare Si (-0.17 V vs. RHE). Figure 3b also shows the dark current densities of the heavily arsenic-doped n<sup>+</sup>-type Si electrodes. In the dark condition, the positive shift in the onset potential of 0.21 V (-0.44 V vs. RHE for N-GQSs/planar Si) also shows higher than that of

Cite this: DOI: 10.1039/c0xx00000x

www.rsc.org/xxxxxx

**ARTICLE TYPE**

planar Si (-0.63 V vs. RHE for planar Si).

When incorporated into the nanostructured photoelectrode system, the N-GQSs exhibited much higher catalytic activity than that of the planar photoelectrode system. The onset potential of the N-GQSs/Si nanowire electrode was 0.26 V vs. RHE, which is 0.09 V higher than that of the Si nanowire without a catalyst (0.17 V vs. RHE). Both the increased onset potential and the current density at the reversible potential (0 V vs. RHE) showed an enhanced ABPE of 2.29%, which is greater than that of the bare Si nanowire system (0.91%). ABPE is the applied bias photon-to-current efficiency.<sup>38</sup>

$$\text{ABPE} = \frac{[j_{\text{ph}} (\text{mA}/\text{cm}^2) \times (V_{\text{redox}} - V_{\text{b}}) (\text{V})]}{P_{\text{in}} (\text{mW}/\text{cm}^2)} \times 100 (\%) \quad (5)$$

where,  $j_{\text{ph}}$  is the photocurrent density obtained under an applied bias  $V_{\text{b}}$ ,  $V_{\text{redox}}$  is the redox potential for hydrogen production (0 V),  $V_{\text{bias}}$  is the externally applied bias potential that is often necessary to achieve reasonable photocurrents, and  $P_{\text{light}}$  is the intensity of the incident light for AM 1.5 G condition (~100 mW/cm<sup>2</sup>). The enhanced photocatalytic performance indicates a synergistic effect between the N-GQSs and Si nanowire structures; moreover, the N-GQSs act as effective HER catalysts on the Si photocathode. Compared to previously reported carbon-based catalysts on Si system, the N-GQSs/Si nanowire system exhibits a higher ABPE.

To investigate the electrocatalytic activity of the N-GQSs, we measured cyclic voltammetry using a rotating disk electrode (RDE) system. To fabricate the working electrode, an N-GQSs solution was transferred to a glassy carbon (GC) tip that was inert in an aqueous solution. As shown in Figure 4a, in the  $J$ - $E$  curves obtained by the RDE measurements, the current density associated with the water splitting reaction exponentially increased after the onset point as the potential was swept from 0.1 V to -0.45 V. For comparison with the potential for the HER in the RDE system, the potential required to attain -5 mA/cm<sup>2</sup> of HER current density was measured for graphene monolayer/GC, N-GQSs/GC, and Pt/GC systems. Also for comparison, the RDE of a graphene monolayer without plasma treatment was measured. The potential required to attain -5 mA/cm<sup>2</sup> of HER current density was -0.32 V vs. RHE for the graphene monolayer without plasma treatment. The potential for the N-GQSs/GC electrode at -5 mA/cm<sup>2</sup> was -0.22 V vs. RHE; this potential was positively (anodically) shifted by 100 mV relative to that for the monolayer graphene. This result indicates that the N-GQSs and monolayer graphene exhibit electrocatalytic activity toward the HER.

To gain further quantitative insight into the catalytic activity of the N-GQSs, the  $J$ - $E$  curves in Figure 4a were converted into plots of the potential as a function of the logarithm of  $J$ . This potential-log  $J$  plot is called a Tafel plot. The measured potentials were corrected for the  $iR$  losses that originated from the resistance of the interface between the electrode and the

electrolyte. Analysis of the impedance spectra revealed that the resistances of the graphene monolayer and N-GQSs/GC were 7.5 and 8.0  $\Omega$ , respectively. The Tafel plot provides two parameters for estimating the electrocatalytic activity: the Tafel slope and the exchange current density. The Tafel slope is defined to be a measure of the potential increase required to increase the resulting current by one order of magnitude. The graphene monolayer exhibited a Tafel slope of 75 mV/decade, and the N-GQSs/GC exhibited a slope of 45 mV/decade, 30 mV lower than that of the graphene monolayer. For comparison with a well-known catalyst, Pt particles were deposited onto GC and the electrocatalytic activity of the resulting electrode was measured. The applied potential required to obtain -5 mA/cm<sup>2</sup> was -0.04 V vs. RHE, which represents a positive shift of 0.18 V relative to that of the N-GQSs/GC electrode. The Tafel slope of Pt-GC was 42 mV/decade, which is similar to that of the N-GQSs/GC. For previously reported carbon-based catalysts, the potential required to attain -5 mA/cm<sup>2</sup> was -0.5 V vs. RHE for N-doped graphene

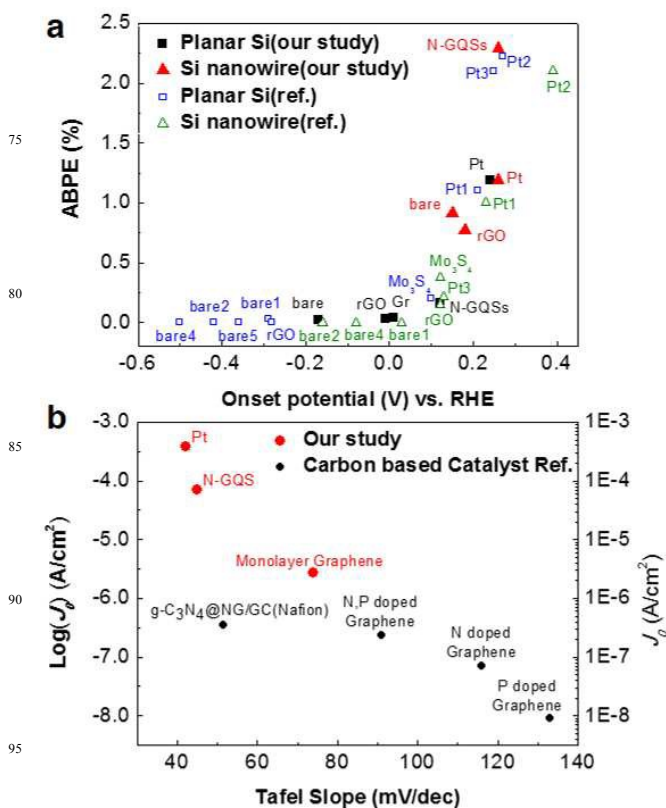


**Figure 5.** Summary of the experimental data for Si and glassy carbon (GC) electrodes. (a) The photoelectrochemical performance of p-type Si-based photoelectrodes. 'Onset potential' and 'ABPE' indicate the potential at -1 mA/cm<sup>2</sup> vs. RHE and the applied bias photon-to-current efficiency, respectively; 'bare' indicates the performance of the bare electrode without deposited catalyst. (b) Electrochemical performance of N-GQSs on GC electrode and other HER catalysts determined using rotating disk electrode system.  $J_0$  indicates that the exchange current

density. References can be found in the supporting information (Tables S2 and S3).

and -0.3 V vs. RHE for graphitic C<sub>3</sub>N<sub>4</sub>, respectively.<sup>23, 24</sup> The Tafel slope was reported to be 116 mV/decade for N-doped graphene and 51.5 mV/decade for graphitic C<sub>3</sub>N<sub>4</sub> when deposited as a mixture with Nafion or carbon black on GC, respectively.

The Tafel slope provides an indication of which reaction steps are possible in the HER among the following:<sup>39</sup>



where H<sub>ads</sub> is adsorbed H, (6) is a discharge step, (7) is a desorption step, and (8) is a recombination step. Considering the adsorbed hydrogen coverage (θ<sub>H</sub>) on the surface of an electrode, if the recombination of adsorbed hydrogen (the Tafel reaction) is the rate-determining step for the HER and if the coverage is very high (θ<sub>H</sub> ≈ 1), the measured Tafel slope will be 30 mV/decade. However, if the electrochemical desorption step (the Heyrovsky reaction) is the rate-determining step, a Tafel slope of 40-118 mV/decade is measured and is dependent of the value of θ<sub>H</sub> (0-1).<sup>40</sup> The observed Tafel slope of 45 mV/decade in the present work indicates that the kinetics of the HER on the graphene monolayer/GC and N-GQS/GC electrodes is determined by the Heyrovsky reaction.

The exchange current density (*J*<sub>0</sub>) of the N-GQSs catalyst was also analyzed. During hydrogen evolution, the current *I* can be described the following equation:<sup>7</sup>

$$I = -e(r^+ - r^-) \quad (9)$$

where *r*<sup>+</sup> - *r*<sup>-</sup> is the net rate of the electron transfer between the oxidation (4e<sup>-</sup> + 4H<sup>+</sup> ← 2H<sub>2</sub>) and the reduction (4e<sup>-</sup> + 4H<sup>+</sup> → 2H<sub>2</sub>) from Eq. (2). The exchange current is the sum of the forward and backward rates when Eq. (2) is in equilibrium. The ability of a given material to catalyze the HER is usually measured by *J*<sub>0</sub>, which is the rate of hydrogen evolution per surface area at the electrode potential when the reaction is at equilibrium. The *J*<sub>0</sub> is also defined as the current density at zero overpotential. The catalytic effect originates from improvement of the rate of charge transfer at the interface between the electrode and electrolyte or from a decrease in the activation energy barrier for a chemical reaction; these catalytic effects are represented by *J*<sub>0</sub>. A high value of *J*<sub>0</sub> indicates that electron transfer or the adsorption/desorption of protons at the electrode/electrolyte can occur more easily, with a lower kinetic barrier. The value of *J*<sub>0</sub> can be obtained by extrapolating the Tafel plot in Figure 4b and extracting the current density at 0 V vs. RHE. The N-GQSs/GC electrode exhibited an enhanced *J*<sub>0</sub> of 7.1 × 10<sup>-5</sup> A/cm<sup>2</sup>, which was 26.3 times greater than the *J*<sub>0</sub> of monolayer graphene on GC (2.7 × 10<sup>-6</sup> A/cm<sup>2</sup>). The *J*<sub>0</sub> of the N-GQSs was also compared with that of other carbon-based catalysts (Table S3). The reported carbon-based catalysts exhibited a lower *J*<sub>0</sub> than that of our N-GQSs electrode. In addition, a metal-free carbon catalyst doped with nitrogen and phosphorous exhibited a *J*<sub>0</sub> of 2.4 × 10<sup>-7</sup> A/cm<sup>2</sup> and a graphitic C<sub>3</sub>N<sub>4</sub> catalyst with nitrogen-doped graphene exhibited 3.5 × 10<sup>-6</sup> A/cm<sup>2</sup> of *J*<sub>0</sub>.<sup>23, 24</sup>

Figure 5 summarizes the experimental data for the Si and GC electrodes. As shown in Figure 5b, our N-GQSs catalyst exhibited a lower Tafel slope and a higher *J*<sub>0</sub> compared to those of other reported carbon-based HER catalysts. Moreover, considering its role as a co-catalyst on the photoelectrode, the N-GQSs/Si nanowire system exhibited better photoelectrochemical performance in terms of ABPE and onset potential than any other reported catalyst/photoelectrode system (Figure 5a). Using only a non-metal carbon-based catalyst without incorporating a noble

65

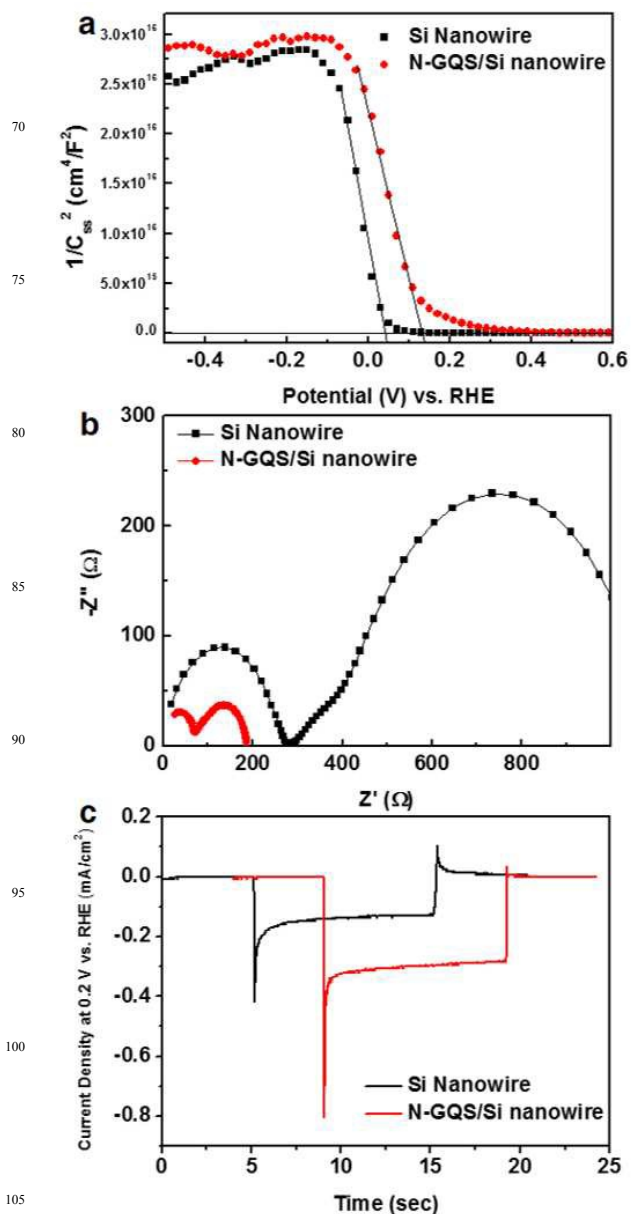


**Figure 6. Comparison of the electrochemical activity of Si nanowire and N-GQSs on Si nanowire.** (a) Mott-Schottky plots from capacitance measurement as a function of potential vs. RHE under dark condition. (b) Nyquist plot for Si nanowire and N-GQSs on Si nanowire at 0 V vs. RHE under dark condition. (c) The transient curve of the photocurrent from Si nanowire and N-GQSs on Si nanowire when the light was turned on and turned off at 0 V vs. RHE.

Cite this: DOI: 10.1039/c0xx00000x

www.rsc.org/xxxxxx

## ARTICLE TYPE

catalyst, the ABPE was increased to 2.29% by the combination of the nanostructured photoelectrode and N-GQSs catalyst. The good HER activity of the N-GQSs is attributed to abundant defects introduced by the plasma treatment. Moreover, high-resolution XPS result show that N-sites are classified into pyridinic (2.07 at%), pyrrolic (0.45 at%), and a small number of quaternary nitrogen (0.16 at%), which acts as the good catalytic sites for HER (Figure S1 e). Previous report also suggested that N-doping on graphene could significantly improve the HER by providing additional active sites<sup>23</sup> and theoretical computation shows favorable N-sites for H adsorption.<sup>41</sup> We are under investigation various N-sites with density functional theory for the precise mechanism on HER.

To further study the electrochemical performance of the N-GQSs/Si electrode, capacitance, impedance, and transient photoresponse measurements were performed, the results of which are shown in Figure 6. Capacitance measurements of the N-GQSs/Si nanowire and bare Si nanowire electrodes were performed as the potential was swept from 0.6 V to -0.5 V vs. RHE in a three-electrode cell without illumination. On the basis of the capacitance results, the flat band potential of the Si nanowire and N-GQSs/Si nanowire electrodes were calculated using the Mott-Schottky relation:<sup>42</sup>

$$1/C_{sc}^2 = 2(E - E_{fb} - kT/e)/(e\epsilon\epsilon_0N) \quad (9)$$

where  $C_{sc}$  is the capacitance of the space charge region,  $\epsilon$  is the dielectric constant of the semiconductor,  $\epsilon_0$  is the permittivity of free space,  $N$  is the donor density (electron donor concentration for an n-type semiconductor or hole acceptor concentration for a p-type semiconductor),  $E$  is the applied potential, and  $E_{fb}$  is the flat band potential. Figure 6a shows the typical Mott-Schottky plots for a p-type silicon semiconductor. The donor density was calculated from the slope, and the  $E_{fb}$  was determined by extrapolation to a capacitance of zero. On the basis of these relations, the N-GQSs/Si nanowire electrode exhibited an  $E_{fb}$  of 0.13 V vs. RHE, whereas the  $E_{fb}$  of the bare Si nanowires was 0.02 V vs. RHE, as shown in Figure 6a. According to the equation:  $E_b = E - E_{fb}$ , the applied potential determines the magnitude of band bending ( $E_b$ ) in the semiconductor and  $E_{fb}$ .<sup>43</sup> As  $E_{fb}$  increases positively, the absolute value of  $E_b$  increases because the applied potential,  $E$  is always negative under the cathodic reaction for proton reduction. Higher band bending at the interface between the electrode and electrolyte promotes faster charge separation of generated electrons and holes.<sup>44</sup> The possibility of charge recombination or surface trapping at sub-band gap energy levels may also be diminished. The higher  $E_{fb}$  of the N-GQSs/SiNW electrode relative to that of the bare SiNW electrode appears to have augmented the extent of band bending at the depletion region of the semiconductor near the solid/solution interface because of the relationship between  $E_b$  and  $E_{fb}$ . Moreover, the doping density of bare SiNW and N-

GQSs/SiNW is also calculated from Mott-Schottky relationship. Using the Eq. (9), the bare SiNW shows the donor density of  $4.46 \times 10^{15} / \text{cm}^3$ , which corresponds to the resistivity of  $10^0 \sim 10^1 \text{ ohm}\times\text{cm}$  for boron doped p-Si.<sup>45</sup> The N-GQSs/SiNW electrodes shows the donor density of  $5.74 \times 10^{15} / \text{cm}^3$ . From the donor density results, N-GQSs deposited on SiNW showed slight increase of the donor density, which might change the electrochemical property at the semiconductor/liquid interface. Zheng *et al.* reported that N dopant adjacent to C atom in a graphene matrix act as an electron acceptor through the analysis of the natural bond orbital population.<sup>23</sup> Likewise, N dopant on GQSs might also act as an active catalytic site for HER.

Impedance measurements were also performed to study the enhanced electrochemical properties of the N-GQSs/SiNW system. Under an illumination intensity of  $100 \text{ mW}/\text{cm}^2$  with a frequency of  $10^3$ -1 Hz and an amplitude of 5 mV in a three electrode system, electrochemical impedance spectroscopy was performed at 0 V vs. RHE. Figure 6b shows a Nyquist plot representing a typical impedance result. In Figure 6b, the N-GQSs/SiNW electrode shows two semicircles that are smaller than those exhibited by the Si nanowire electrode. On the basis of the results gathered from these two semicircles, two capacitance elements can be assigned: the capacitance of the charge depletion layer in the semiconductor and the capacitance of the double layer at the semiconductor/electrolyte interface. In the high-frequency region, the charge transfer process in the depletion layer of the semiconductor dominates, whereas charge transfer across the double layer at the semiconductor/electrolyte interface is dominant in the low-frequency region.<sup>46</sup> In the case of the N-GQSs/SiNW electrodes, the two semicircles indicating charge transfer processes in the double layers at the solid/solution interface and in the depletion region of the semiconductor are smaller than those of the bare SiNWs. The smaller semicircle in the low frequency range means that the charge transfer resistance of the N-GQSs/SiNW in the double layer is lower than that of bare SiNW. The charge transfer resistance is also related with a kinetic barrier energy for the faradaic reactions across the double.<sup>46</sup> Thus, N-GQSs might promote the faradaic reactions by reducing the charge transfer resistance across the double layer. Similar charge transfer mechanism of the hydrogen production was also reported using reduced graphene oxide catalyst.<sup>28</sup> From the result of smaller semicircle in the high frequency range, the charge transfer resistance of the semiconductor depletion layer in the N-GQSs/SiNW is also lower than that of the bare SiNW. The charge transfer resistance in the semiconductor depletion layer is also correlated with higher photocurrent response because of the higher band bending in the depletion layer.<sup>44, 47</sup>

Transient photoresponse measurements were also performed to determine the factors enhancing the photoelectrochemical performance of the N-GQSs/SiNW electrodes; the results are shown in Figure 6c. The transient behavior of the N-GQSs/SiNW and bare Si nanowire electrodes was measured at 0.2 V vs. RHE using a chopped illumination system. Figure 6c shows the

transient behavior of the N-GQSs/Si and bare Si electrodes without a catalyst. The light was turned on and turned off after 10 sec while the potential was maintained at 0.2 V vs. RHE. At the moment of the light was turned on, the current density reached a peak, which is referred to as the initial photocurrent density ( $J_{in}$ ). The  $J_{in}$  values of the N-GQSs/Si nanowire and bare Si nanowire electrodes were  $-0.80 \text{ mA/cm}^2$  and  $-0.42 \text{ mA/cm}^2$ , respectively. The current density then saturated, and the saturated photocurrent density ( $J_{st}$ ) under illumination was  $-0.30 \text{ mA/cm}^2$  for the N-GQSs/Si nanowire electrode and  $-0.13 \text{ mA/cm}^2$  for the bare Si nanowire electrode. At the moment the light was turned off, the current density again showed an oscillating plot, and the current density at the peaks was designated as  $J_{off}$ . The  $J_{off}$  values of the N-GQSs/Si nanowire and Si nanowire electrodes were  $-0.02 \text{ mA/cm}^2$  and  $-0.12 \text{ mA/cm}^2$ , respectively. The high  $J_{st}/J_{in}$ , N-GQSs ratio of 0.375 and small  $J_{off}$  of the N-GQS/Si nanowire electrode suggest that fewer carriers were trapped and that less recombination occurred at the surface state of the electrode surface, in comparison with those of the surface state of the bare Si nanowire sample ( $J_{st}/J_{in, \text{bare}} = 0.309$ ). Together, the capacitance and impedance results indicate that the N-GQSs/Si nanowire electrode can contribute to charge separation by inducing favorable band bending and boosting the charge transfer rate, which enhance the electrode's HER performance. To summarize, the results obtained from the capacitance, impedance, and transient photoresponse measurements indicate that the N-GQSs/SiNW electrode enhances the HER activity by reducing the possibility of charge recombination and lowering the kinetic barriers for the HER at the interface between the Si semiconductor and electrolyte solution.

## Conclusion

We fabricated N-doped graphene quantum sheets (N-GQSs) as a catalyst for the solar-driven hydrogen evolution reaction on Si nanowire photocathodes. The onset potential for the Si nanowire photocurrent was significantly shifted toward the anodic direction without a change in the saturation current density. N-GQSs exhibited excellent catalytic activity for the photoelectrochemical HER on Si nanowire photocathodes. The results showed that the N-GQSs electrodes exhibited a ABPE of 2.29%, which is higher than that of any other carbon-based photoelectrochemical HER catalysts reported to date. Our approach in this study involved a strategy for developing metal-free carbon-based catalysts with high efficiency for solar-driven hydrogen fuel production.

## Experimental

### Synthesis of graphene quantum sheets

A copper foil ( $10 \times 10 \text{ cm}^2$ ) was inserted into a quartz tube and then heated to  $1,000^\circ\text{C}$  min with flowing 5 sccm  $\text{H}_2$ . After reaching  $1,000^\circ\text{C}$ , the sample was annealed for 20 min under the same condition. The gas mixture of 50 sccm  $\text{CH}_4$  and 5 sccm  $\text{H}_2$  was flowed for 30 min at a pressure of 8 Torr. After growth, the monolayer graphene on back-side of copper was removed by oxygen plasma (100 W RF power, 12 sec). Next, the N-GQSs were prepared by being irradiate with nitrogen plasma (10 W RF power, 12 sec) to graphene on front-side of copper foil. Finally, the N-GQSs were floated on a 0.1 M ammonium persulfate etchant to remove the Cu substrate. After the Cu was removed,

the floating N-GQSs were dispersed in a common organic solvent such as dichloromethane by solvent extraction.<sup>48</sup>

### Preparation of Si nanowire (SiNW) photocathode

Boron-doped (p-type) single-crystal Si wafers (4-inch diameter, 500- $\mu\text{m}$  thickness, doped to achieve a resistivity of 10-15  $\Omega\text{cm}$ , oriented along the (100) plane were purchased from Namkang Co. Ltd.  $\text{AgNO}_3$  powder (99.5%) and HF (48-51 wt%) were purchased from Sigma Aldrich, and concentrated nitric acid solution (70 wt%) was purchased from Daejung Chemical. The wafers were cut into  $1 \text{ cm}^2$  pieces and successively cleaned in acetone, 2-propanol and deionized water for 10 min under sonication.

Each of the Si nanostructures was fabricated by the metal-catalyzed electroless etching method in a 20 mL aqueous solution of  $\text{AgNO}_3$  (0.015 M) and HF (5 M) for an etching times of 20 min, 30 min, 120 min, or 180 min (Figure S5). Excess Ag residues that could be contaminated during the electroless etching were removed by washing with 70% nitric acid solution for two hours.

A SiNW photocathode was fabricated by establishing an ohmic contact at the back side of a Si substrate. After a native oxide layer was removed on the Si surface using HF, gallium-indium eutectic alloy was loaded onto the surface, followed by the application of silver conductive paste a copper wire; the resulting assembly was then dried at  $100^\circ\text{C}$ . To insulate and protect the back contact of the Si substrate, epoxy was applied over the entire sample except for the area that was illuminated on the front side. After the bare Si cell was fabricated, N-GQSs were transferred onto the Si surface via drop-casting.

### Electrochemical measurements

Photoelectrochemical measurements were performed in a three-electrode cell using an electrochemical analyzer (CHI 760E, CH Instruments, Inc.). Schematic illustration and photograph images of hydrogen evolution reaction on N-GQSs/Si photocathode are shown in Figure S6. Pt foil and Pt wire were used as the counter electrode, and a  $\text{Ag}/\text{AgCl}/3 \text{ M NaCl}$  electrode was used as the reference electrode. The reference electrode was carefully calibrated with respect to RHE at  $25^\circ\text{C}$  in an aqueous 1 M perchloric acid solution saturated with high purity  $\text{H}_2$ . The RHE was calibrated to between  $-0.201 \text{ V}$  and  $-0.203 \text{ V}$  vs. the  $\text{Ag}/\text{AgCl}$  reference electrode (Figure S7). To evaluate the photoelectrochemical behavior, visible light from a 300 W Xe lamp was illuminated onto the substrate with a light intensity of  $100 \text{ mW/cm}^2$  using a glass Air Mass 1.5 Global filter. For the electrochemical study, the Rotating Disk Electrode (RDE) system was purchased from PINE, Inc., and a glass carbon tip was used for the RDE measurements (dia. 5 mm). For comparison, 10  $\mu\text{L}$  of Pt catalyst ink mixed with 5 wt% Nafion was loaded onto the GC and dried at  $110^\circ\text{C}$ . RDE measurements were performed at a rotation speed of 1,000 rpm and at a scan rate of 5 mV/sec.

### Characterization

Raman spectra were collected using a Renishaw micro-Raman spectrometer with an excitation wavelength of 514.5 nm emitted from an Ar laser. The spot diameter was  $\sim 2 \mu\text{m}$ , and a  $50\times$  objective lens was used. Oxygen plasma treatment (SNTEK) was carried out at a radio-frequency (rf) power of 100 W for 13 sec under a pressure of 140 mTorr for back side of graphene on Cu and the nitrogen plasma was accelerated at an rf power of 10 W over an exposure time of 12 sec under a pressure of 120 mTorr on

Cite this: DOI: 10.1039/c0xx00000x

www.rsc.org/xxxxxx

## ARTICLE TYPE

graphene.

## Notes and references

<sup>a</sup> Department of Materials Science & Engineering, Seoul National University, 1 Gwanak-ro, Gwanak-gu, Seoul, 151-744, Korea, Tel: 82-2-880-8305; E-mail: [nkita@snu.ac.kr](mailto:nkita@snu.ac.kr)

<sup>b</sup> Department of Chemistry, Seoul National University, 1 Gwanak-ro, Gwanak-gu, Seoul, 151-744, Korea, Tel: 82-2-880-6559; E-mail: [byunghee@snu.ac.kr](mailto:byunghee@snu.ac.kr)

<sup>c</sup> National Center for Inter-University Research Facilities, Seoul National University, 1 Gwanak-ro, Gwanak-gu, Seoul, 151-744, Korea

<sup>d</sup> Graduate School of Convergence Science and Technology, Seoul National University, Suwon 443-270, Korea.

† Electronic Supplementary Information (ESI) available: Additional information, figures, and table. See DOI: 10.1039/b000000x/

‡ These authors contributed equally to this work.

## Acknowledgment

This research was supported by the Basic Science Research Program (2011-0011225, 2011-0017587, 2012M3A7B4049807), the Global Frontier R&D Program of the Center for Multiscale Energy System (2011-0031574), the Global Research Lab (GRL) Program (2011-0021972), and the Fusion Research Program for Green Technologies through the National Research Foundation of Korea (2012M3C1A1048863), funded by the Ministry of Science, ICT & Future, Korea. This research was also supported by the Ministry of Science, ICT & Future, through the Research Institute of Advanced Materials (RIAM).

## References

1. J. A. Turner, *Science*, 2004, 305, 972-974.
2. N. S. Lewis and D. G. Nocera, *Proceedings of the National Academy of Sciences*, 2006, 103, 15729-15735.
3. M. G. Walter, E. L. Warren, J. R. McKone, S. W. Boettcher, Q. Mi, E. A. Santori and N. S. Lewis, *Chemical Reviews*, 2010, 110, 6446-6473.
4. T. R. Cook, D. K. Dogutan, S. Y. Reece, Y. Surendranath, T. S. Teets and D. G. Nocera, *Chemical Reviews*, 2010, 110, 6474-6502.
5. S. W. Boettcher, E. L. Warren, M. C. Putnam, E. A. Santori, D. Turner-Evans, M. D. Kelzenberg, M. G. Walter, J. R. McKone, B. S. Brunschwig, H. A. Atwater and N. S. Lewis, *Journal of the American Chemical Society*, 2011, 133, 1216-1219.
6. U. Sim, H.-Y. Jeong, T.-Y. Yang and K. T. Nam, *Journal of Materials Chemistry A*, 2013, 1, 5414-5422.
7. J. K. Nørskov, T. Bligaard, A. Logadottir, J. R. Kitchin, J. G. Chen, S. Pandalov and U. Stimming, *Journal of The Electrochemical Society*, 2005, 152, J23-J26.
8. T. F. Jaramillo, J. Bonde, J. Zhang, B.-L. Ooi, K. Andersson, J. Ulstrup and I. Chorkendorff, *The Journal of Physical Chemistry C*, 2008, 112, 17492-17498.
9. Y. Hou, A. B. Laursen, J. Zhang, G. Zhang, Y. Zhu, X. Wang, S. Dahl and I. Chorkendorff, *Angewandte Chemie International Edition*, 2013, 52, 3621-3625.
10. Y. Yan, B. Xia, Z. Xu and X. Wang, *ACS Catalysis*, 2014, 4, 1693-1705.
11. C. Chen, Y. Kang, Z. Huo, Z. Zhu, W. Huang, H. L. Xin, J. D. Snyder, D. Li, J. A. Herron, M. Mavrikakis, M. Chi, K. L. More, Y. Li, N. M. Markovic, G. A. Somorjai, P. Yang and V. R. Stamenkovic, *Science*, 2014, 343, 1339-1343.
12. J. R. McKone, E. L. Warren, M. J. Bierman, S. W. Boettcher, B. S. Brunschwig, N. S. Lewis and H. B. Gray, *Energy & Environmental Science*, 2011, 4, 3573-3583.
13. B. Marsen, B. Cole and E. L. Miller, *Solar Energy Materials and Solar Cells*, 2008, 92, 1054-1058.
14. M. W. Kanan, Y. Surendranath and D. G. Nocera, *Chemical Society Reviews*, 2009, 38, 109-114.
15. A. Kudo and Y. Miseki, *Chemical Society Reviews*, 2009, 38, 253-278.
16. J. Ran, J. Zhang, J. Yu, M. Jaroniec and S. Z. Qiao, *Chemical Society Reviews*, 2014, 43, 7787-7812.
17. I. Oh, J. Kye and S. Hwang, *Nano Letters*, 2011, 12, 298-302.
18. D. H. Youn, S. Han, J. Y. Kim, J. Y. Kim, H. Park, S. H. Choi and J. S. Lee, *ACS Nano*, 2014, 8, 5164-5173.
19. R. K. Shervedani and A. Lasia, *Journal of The Electrochemical Society*, 1998, 145, 2219-2225.
20. B. Cao, G. M. Veith, J. C. Neufeld, R. R. Adzic and P. G. Khalifah, *Journal of the American Chemical Society*, 2013, 135, 19186-19192.
21. S. Chen, J. Duan, Y. Tang, B. Jin and S. Zhang Qiao, *Nano Energy*, 2015, 11, 11-18.
22. K. S. Novoselov, A. K. Geim, S. V. Morozov, D. Jiang, M. I. Katsnelson, I. V. Grigorieva, S. V. Dubonos and A. A. Firsov, *Nature*, 2005, 438, 197-200.
23. Y. Zheng, Y. Jiao, L. H. Li, T. Xing, Y. Chen, M. Jaroniec and S. Z. Qiao, *ACS Nano*, 2014, 8, 5290-5296.
24. Y. Zheng, Y. Jiao, Y. Zhu, L. H. Li, Y. Han, Y. Chen, A. Du, M. Jaroniec and S. Z. Qiao, *Nat Commun*, 2014, 5.
25. Y. Liang, Y. Li, H. Wang, J. Zhou, J. Wang, T. Regier and H. Dai, *Nat Mater*, 2011, 10, 780-786.
26. J.-D. Qiu, G.-C. Wang, R.-P. Liang, X.-H. Xia and H.-W. Yu, *The Journal of Physical Chemistry C*, 2011, 115, 15639-15645.
27. Q. Xiang, J. Yu and M. Jaroniec, *Chemical Society Reviews*, 2012, 41, 782-796.
28. Z. Huang, P. Zhong, C. Wang, X. Zhang and C. Zhang, *ACS Applied Materials & Interfaces*, 2013, 5, 1961-1966.
29. U. Sim, T.-Y. Yang, J. Moon, J. An, J. Hwang, J.-H. Seo, J. Lee, K. Y. Kim, J. Lee, S. Han, B. H. Hong and K. T. Nam, *Energy & Environmental Science*, 2013, 6, 3658-3664.
30. Y. Hou, B. L. Abrams, P. C. K. Vesborg, M. E. Björketun, K. Herbst, L. Bech, A. M. Setti, C. D. Damsgaard, T. Pedersen, O. Hansen, J. Rossmeisl, S. Dahl, J. K. Nørskov and I. Chorkendorff, *Nat Mater*, 2011, 10, 434-438.
31. Y. W. Chen, J. D. Prange, S. Dühren, Y. Park, M. Gunji, C. E. D. Chidsey and P. C. McIntyre, *Nat Mater*, 2011, 10, 539-544.
32. J. Oh, T. G. Deutsch, H.-C. Yuan and H. M. Branz, *Energy & Environmental Science*, 2011, 4, 1690-1694.
33. B. M. Kayes, H. A. Atwater and N. S. Lewis, *Journal of Applied Physics*, 2005, 97, -.
34. D. B. Williams, Carter, C. Barry, *Transmission Electron Microscopy*, Springer, 2009.
35. K. Peng, H. Fang, J. Hu, Y. Wu, J. Zhu, Y. Yan and S. Lee, *Chemistry – A European Journal*, 2006, 12, 7942-7947.
36. E. Garnett and P. Yang, *Nano Letters*, 2010, 10, 1082-1087.
37. L. Tsakalakos, J. Balch, J. Fronheiser, M.-Y. Shih, S. F. LeBoeuf, M. Pietrzykowski, P. J. Codella, B. A. Korevaar, O. V. Sulima, J. Rand, A. Davuluru and U. Rapol, *NANOP*, 2007, 1, 013552-013552-013510.
38. Z. Chen, T. F. Jaramillo, T. G. Deutsch, A. Kleiman-Shwarsstein, A. J. Forman, N. Gaillard, R. Garland, K. Takanabe, C. Heske, M. Sunkara, E. W. McFarland, K. Domen, E. L. Miller, J. A. Turner and H. N. Dinh, *Journal of Materials Research*, 2010, 25, 3-16.
39. L. R. F. Allen J. Bard, *John Wiley & Sons, Inc.*, 2001, 864.
40. B. E. Conway and G. Jerkiewicz, *Electrochimica Acta*, 2000, 45, 4075-4083.
41. Y. Fujimoto and S. Saito, *Journal of Applied Physics*, 2014, 115, 153701-1-153701-5.
42. A. W. Bott, *Current Separations*, 1998, 17, 87-91.

43. K. Gelderman, L. Lee and S. W. Donne, *Journal of Chemical Education*, 2007, 84, 685.
44. N. S. Lewis, *Journal of The Electrochemical Society*, 1984, 131, 2496-2503.
- 5 45. R. E. Hummel, *Electronic Properties of Materials*, Springer, 4th edn., 2011.
46. D. Merki, H. Vrubel, L. Rovelli, S. Fierro and X. Hu, *Chemical Science*, 2012, 3, 2515-2525.
47. T. Lopes, L. Andrade, H. A. Ribeiro and A. Mendes, *International Journal of Hydrogen Energy*, 2010, 35, 11601-11608.
- 10 48. J. Moon, J. An, U. Sim, S.-P. Cho, J. H. Kang, C. Chung, J.-H. Seo, J. Lee, K. T. Nam and B. H. Hong, *Advanced Materials*, 2014, 26, 3501-3505.

15

Cite this: DOI: 10.1039/c0xx00000x

www.rsc.org/xxxxxx

ARTICLE TYPE

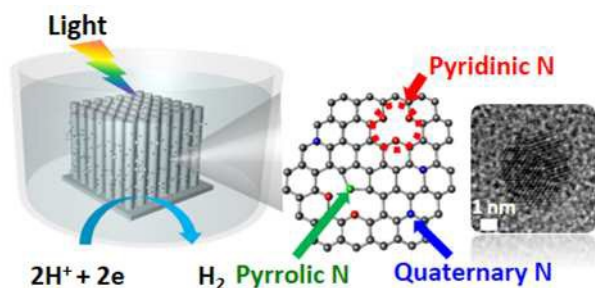


### Table of Contents

N-doped graphene quantum sheets decorated on a Si nanowire photocathode electrode serve as an efficient electrocatalyst for photoelectrochemical hydrogen production.

### Broader Text

Hydrogen production by solar energy has been widely studied as an environmentally friendly and sustainable energy source. Silicon-based electrodes can serve as photocathodes for hydrogen production under visible light because of their appropriate band structures. However, kinetic issues regarding the exchange current require an overpotential and the use of catalysts in the system. The development of catalysts for hydrogen production is of fundamental and technological importance. To solve the problems associated with previously reported noble metal-based catalysts, carbon-based catalysts serve as an important research direction in the search for low-cost, environmentally friendly, and corrosion-resistant catalysts. In this work, we fabricated graphene quantum sheets as a catalyst on Si nanowire photocathodes for the solar-driven hydrogen evolution reaction. Our approach in this study exploits a strategy for developing metal-free carbon-based catalysts with high efficiency for solar-driven hydrogen fuel production.